Erschienen in: SiliconPV, the 8th International Conference on Crystalline Silicon Photovoltaics / Ballif, Christopher (Hrsg.). - Melville, NY : AIP Publishing, 2018. - (AIP Conference Proceedings ; 1999,1). - 130013. - ISBN 978-0-7354-1715-1
https://dx.doi.org/10.1063/1.5049332

Light-Induced Degradation Variation in Industrial Multicrystalline PERC Silicon Solar Cells

Jeanette Lindroos[1, a)], Annika Zuschlag[1, b)], Jürgen Carstensen[2, c)], and Giso Hahn[1, d)]

[1]*University of Konstanz, Universitätsstr. 10, 78464 Konstanz, Germany.*
[2]*Christian-Albrechts University of Kiel, Kaiserstr. 2, 24143 Kiel, Germany.*

[a)]Corresponding author: jeanette.lindroos@alumni.aalto.fi
[b)]annika.zuschlag@uni-konstanz.de
[c)]jc@tf.uni-kiel.de
[d)]giso.hahn@uni-konstanz.de

Abstract. Light and elevated temperature induced degradation (LeTID) varies significantly in multicrystalline PERC silicon solar cells, depending mainly on the solar cell processes. We show that despite high firing temperatures, LeTID can manifest itself in two different ways: 1) strong LeTID in good grains (j_{sc} and V_{oc} losses >7%$_{rel.}$), or 2) low LeTID in good grains with stronger LeTID at dislocation clusters. Such LeTID at dislocation clusters is not only caused by a bulk recombination increase but also by an increased back-surface recombination velocity.

INTRODUCTION

Light and elevated temperature induced degradation (LeTID) varies in multicrystalline (mc) Passivated Emitter and Rear Cells (PERC) silicon solar cells from less than 1%$_{rel.}$ to above 10%$_{rel.}$, depending on the wafer bulk and the solar cell processing [1-8]. LeTID formation is particularly sensitive to the peak temperature [3] and the cooling profile of the firing step [4]. PERC cells that have been fired above 675°C [3] and cooled down rapidly show strong homogenous LeTID in the mc grains, with lower defect densities at the grain boundaries [6]. Slower cooling in RTP furnaces has resulted in less but still homogenous degradation [4]. Lifetime sample studies have also revealed that the surface passivation layer impacts the LeTID defect density [7,8]. As many surface passivation layers are unstable under LeTID formation conditions [9], back-surface passivation degradation might occur in mc-PERC cells during illumination.

In order to understand why cell degradation varies between different PERC processes, we perform spatially resolved analysis of mc-PERC cells with weak and strong LeTID. We separate bulk degradation from back-surface passivation changes, and investigate a possible link to the surface passivation deposition.

EXPERIMENTAL

In the first experiment, 1 Ωcm B-doped high-performance mc-Si sister wafers from the middle of the ingot were subjected to two different industrial PERC processes (A & B). The cells were fired in a belt furnace at different firing temperatures above 675°C. After processing, the initial state was mapped with Photoluminescence (PL), Light Beam Induced Current (LBIC), and CELLO [10,11]. During PL measurements, the cells were illuminated with a 808 nm laser at 1 sun [12]. LBIC was mapped at a spatial resolution of 50 µm with a LOANA tool [13] at seven wavelengths (405-980 nm).

CELLO mapping was performed at a spatial resolution of 200 µm with three lasers (660, 830, and 934 nm), each of which at four lock-in modulation frequencies (6.05, 9.35, 17.05, and 20.35 kHz). The resulting amplitude and phase shift maps (24 in total) were fitted to a model of an ohmic resistance in series to the light-wavelength-dependent short-

SiliconPV 2018, The 8th International Conference on Crystalline Silicon Photovoltaics
AIP Conf. Proc. 1999, 130013-1–130013-7; https://doi.org/10.1063/1.5049332
Published by AIP Publishing. 978-0-7354-1715-1/$30.00

circuit current. The short-circuit current was calculated from the diffusion equation combining minority carrier diffusion, bulk recombination, and surface recombination at the backside. Mixing data of three lasers with different penetration depth caused unavoidably differences in the injection level throughout the thickness of the solar cell. These injection level differences were taken into account by an additional fitting parameter, which will not be discussed further in this paper.

The cells were illuminated with 0.9±0.1 suns under open-circuit conditions at 75±3°C, and the degradation was monitored by regular I-V measurements at standard conditions. Once the cells had reached near full degradation, the illumination was stopped, and the degraded state was again characterized with PL, LBIC, and CELLO.

The second experiment was performed on a 5x5 cm^2 sample that was cut out of a sister wafer. After saw-damage etching and cleaning, double-sided SiN_x:H (75 nm) was deposited with an inductively-coupled plasma (ICP) PECVD tool, similar to the one used in PERC B processing. After firing at a set T of 800°C, the SiN_x:H layer was removed and replaced with iodine ethanol (IE) passivation. The minority carrier recombination lifetime was then measured with time-resolved photoluminescence imaging (TR-PLI) [14,15]. After the initial measurement, the IE was removed, and the bare sample was subjected to 0.9±0.1 sun illumination at 150°C for 24 h. Finally, the sample was passivated with fresh IE, and the degraded lifetime was measured with TR-PLI.

RESULTS AND DISCUSSION

In both industrial PERC processes, the solar cells were fired above 675°C. Nevertheless, the cells degrade very differently. PERC A shows expectedly strong LeTID with j_{sc} and V_{oc} losses of ≥ 7 $\%_{rel.}$ in Fig. 1, whereas PERC B degrades only by 0.9 $\%_{rel.}$ in j_{sc} and 0.6 $\%_{rel.}$ in V_{oc}. In both cells, the j_{sc} losses are larger than the V_{oc} degradation, which means that the LeTID differences can be analysed in more detail by spatially resolved LBIC. Figures 2a)-f) show the IQE maps of a PERC A area measured in the initial and degraded states with LBIC. In maps 2a)-c), the IQE signal at 830 nm is dominated by bulk recombination, whereas the 980 nm laser penetrates deep enough for j_{sc} to be reduced by back-surface recombination. At both wavelengths in Figs. 1c) and f), PERC A exhibits typical LeTID distribution: homogenous degradation in good areas of the grains, with weaker LeTID at grain boundaries [6]. In addition, PERC A shows lower LeTID at recombination-active dislocation clusters, which is observed also in the reference PL map in Fig. 1i). The drawbacks of these mapping methods are the imprecise injection levels, which vary over different grain structures and between the two measurement states. Nevertheless, injection-controlled lifetime studies have confirmed zones of denuded LeTID around the grain boundaries [16] but reported higher defect densities at dislocation clusters compared with homogenous grain degradation [16,17].

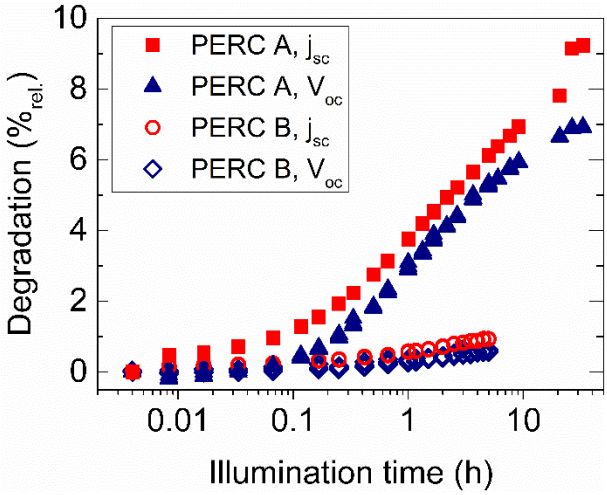

FIGURE 1. Relative degradation of j_{sc} and V_{oc} in PERC cells A and B during 0.9±0.1 sun illumination at 75±3°C.

Figure 3 displays the corresponding IQE and PL maps of PERC B, along with LeTID comparison maps. After both IQE and PL analysis, PERC B shows very different spatial degradation compared with PERC A. In PERC B, the strongest degradation is measured at recombination-active dislocation clusters, whereas the good grains areas show only low LeTID. The IQE comparison maps of LeTID in Fig. 3j) shows that LeTID at the dislocation clusters in PERC B is more severe than in PERC A, even though PERC A degrades more in the good grain regions. On the other hand, when LeTID in the two cells is compared by PL mapping in Fig. 3k), PERC A degrades more than PERC B in both the good grains and at dislocation clusters.

The inhomogeneous LeTID in PERC B resembles dislocation-related LID observed in mc-Si Al-BSF with low-injection LBIC at 830 nm, after 1 sun illumination at 40°C [18]. As these Al-BSF cells were manufactured by entirely different processes than PERC B, it is probably just a coincidence that lowly degrading Al-BSF cells show similar spatial LID distribution as PERC B with weak LeTID. Luckily, PERC B was mapped at several LBIC wavelengths. Degradation in the good grains is observed only when $\lambda \geq 940$ nm, which is also when back-surface recombination clearly starts to decrease the IQE signal. Furthermore, LeTID-denuded zones only appear around grain boundaries in the IQE map at 980 nm, which is heavily affected by back-surface recombination. Therefore, LeTID in PERC B might be linked to changes in the back-surface passivation. In order to separate between back-surface and bulk recombination, we perform CELLO mapping on both PERC A and B.

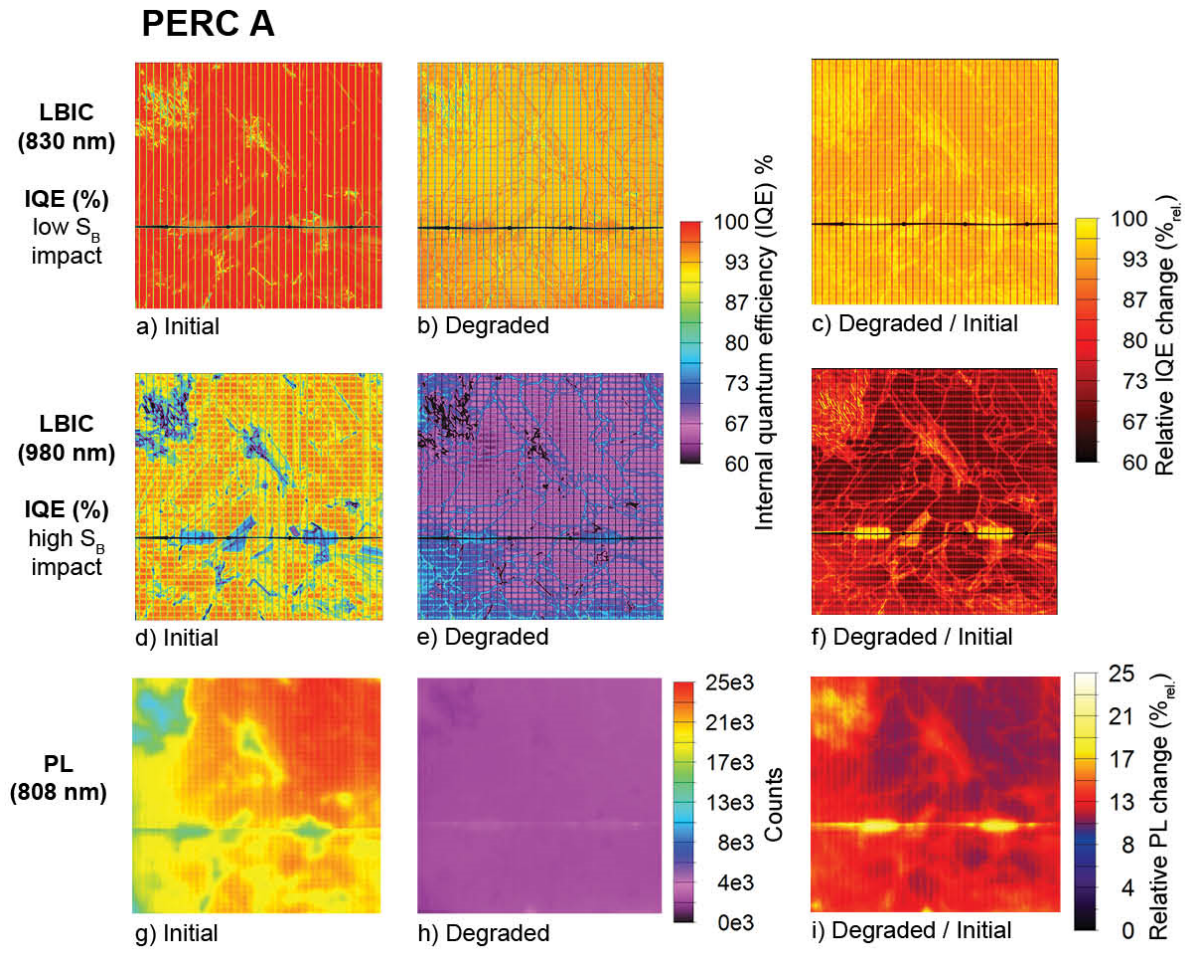

FIGURE 2. 5x5 cm^2 maps from PERC A measured with LBIC at 830 and 980 nm (a-f), along with PL at 808 nm (g-i) before (Initial) and after (Degraded) 33 h of illumination. Maps c), f) and i) show the relative degradation, where 100 %$_{rel.}$ indicates no signal change.

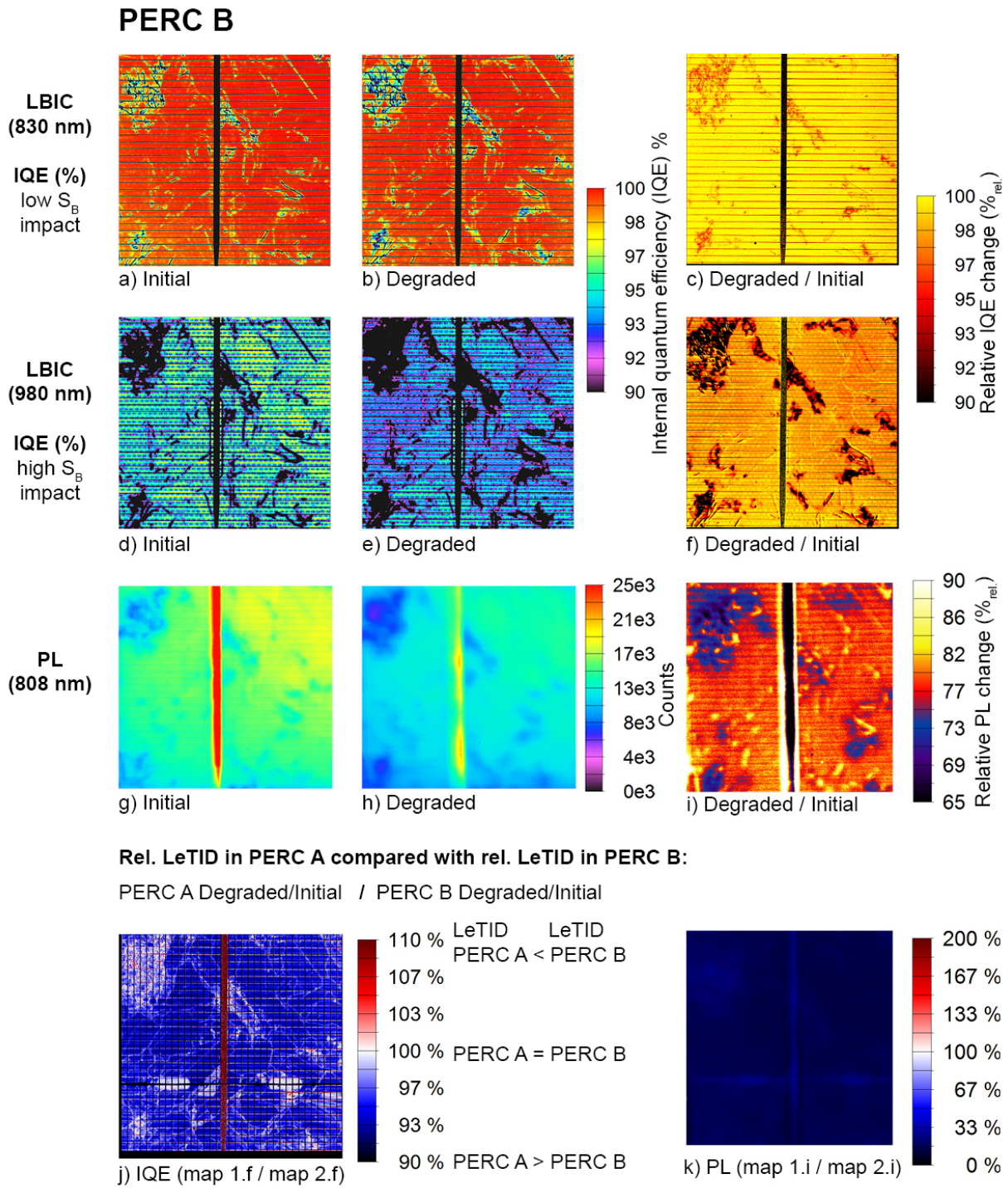

FIGURE 3. 5x5 cm^2 maps from PERC cell B measured with LBIC at 830 and 980 nm (a-f), along with PL at 808 nm (g-i) before (Initial) and after (Degraded) 5 h of illumination. Maps c), f) and i) show the relative degradation, where 100 %$_{rel.}$ indicates no signal change. Maps j) and k) show the relative LeTID of PERC A compared with PERC B using IQE and PL.

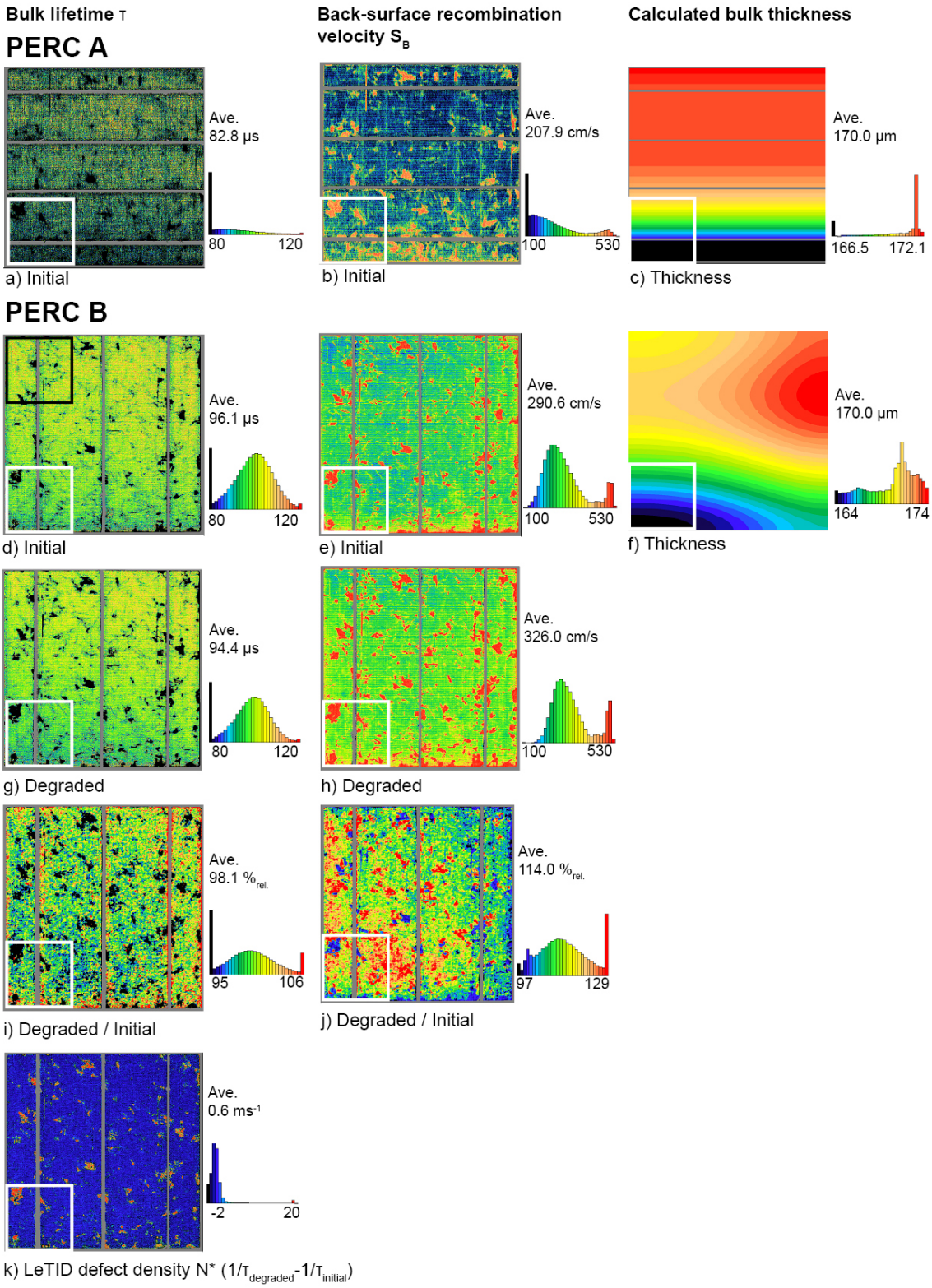

FIGURE 4. Bulk lifetime (a, d & g), back-surface recombination velocity (b, e & h), and bulk thickness maps (c & f) of the initial and the degraded PERC A and B, extracted from CELLO measurements. Maps i) & j) show the relative degradation. Map k) displays the normalized LeTID defect density in PERC B. The white squares show the positions of Figs. 2 & 3, and the black one in map d) indicates the location of Fig. 5.

Figure 4 shows the bulk lifetime and back-surface recombination velocity (S_B) maps of PERC A and B extracted from the CELLO measurements. The analysis takes into account the bulk thickness variations over the cells, shown in Figs. 4c) and f). In the good grain areas, Fig. 4a shows lower bulk lifetime in PERC A compared with PERC B in Fig. 4d. On the other hand, PERC A has better back-surface passivation, as the back-surface recombination velocity is lower in Fig. 4b compared with PERC B in Fig. 4e). In both cells, many dislocation clusters show not only high bulk recombination but also higher back-surface recombination, than the good grain areas. High S_B values at dislocation clusters correspond to previous CELLO results on mc-Si Al-BSF solar cells [10,11]. It might be caused by reduced chemical passivation, due to a higher density of dangling bonds in the interface between the dislocated bulk and the passivation layer.

After illumination, Figs. 4g) and h) display the bulk lifetime and S_B maps of the degraded PERC B. As expected from Fig. 3, illumination causes a clear decrease in the bulk lifetime at dislocation-clusters in Fig. 4i). The good areas hardly degrade, except for the thinnest parts of the cell. Nevertheless, the LeTID defect density map in Fig. 4k) shows that change is negligible compared with bulk LeTID formation at dislocation clusters. Figure 4j) shows a slight S_B increase over the whole cell with higher changes in good grain regions of the thinnest cell areas. The largest S_B changes are measured at/near many of the dislocation clusters that also show the largest decrease in bulk lifetime. Hence, the stronger LeTID measured at dislocation clusters in PERC B is in some cases a cumulative effect of both increased bulk and back-surface recombination. The degraded PERC A is dominated so strongly by bulk recombination that S_B cannot be reliably extracted from CELLO measurements.

Although the two PERC cell processes have different emitter profiles, efficacies of impurity segregation, and peak firing temperatures, these high-temperature process steps cannot alone explain the weak LeTID in PERC B. Recent lifetime data show that the surface passivation layer must be present during the firing steps for LeTID to form during consequent illumination [7,8]. The chosen deposition tool is also shown to play a clear role in LeTID formation [7,8], not just because of differences in the deposited layers [19], but also the deposition temperature [8]. Unfortunately, lifetime samples were not available with the exact passivation layers as used in PERC processes A and B. Nevertheless, Figure 5 shows the lifetime maps and LeTID defect density maps of a sister wafer area, which was subjected to SiN_x:H deposition with a fast ICP-PECVD tool, similar to the one used in PERC B. After full degradation, the effective lifetime in the good grain areas stays above 150 µs in Fig. 5b). The defect density map in Fig. 5c) shows the highest LeTID at dislocation clusters, which corresponds to PERC B degradation in Fig. 3. As many previous lifetime studies have observed the strongest LeTID at dislocation clusters (regardless of LeTID defect density in the good grains) [8,16,17], the SiN_x:H deposition affects LeTID mostly by reducing the defect density in the good grain areas. Furthermore, the lifetime sample shows no difference between LeTID at grain boundaries and in good grain areas, which corresponds to the IQE and PL maps of PERC B in Fig. 3. Since a mere decrease of the firing temperature does not erase the difference between LeTID in good grains and at grain boundaries [20], the weak LeTID in PERC B might be linked to the surface passivation deposition.

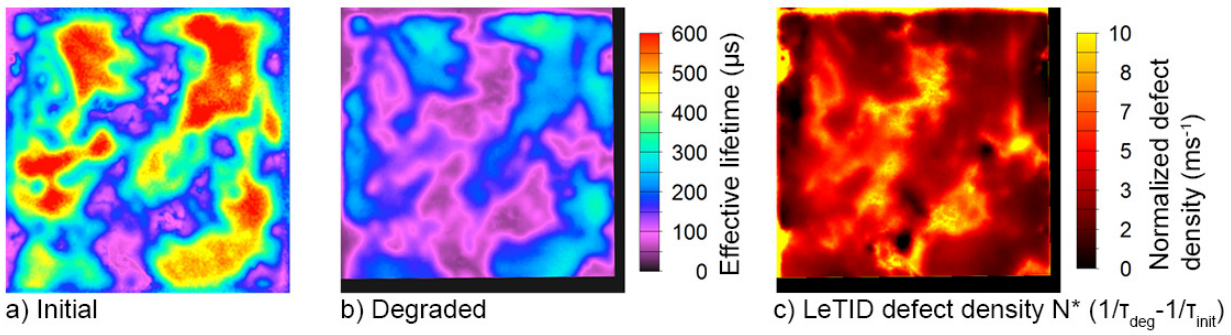

FIGURE 5. TR-PLI lifetime maps of a sample fired with SiN_x:H measured with IE passivation in a) the initial and b) the degraded state. Map c) shows the normalized LeTID defect density.

CONCLUSIONS

Sister wafers subjected to two different PERC processes degrade very differently during illumination at 75°C. PERC A suffers from j_{sc} and V_{oc} losses of over 7 $\%_{rel.}$ during 33 h of illumination, whereas LeTID in PERC B saturates at a j_{sc} loss of 0.9 $\%_{rel.}$ and V_{oc} loss of 0.6 $\%_{rel.}$ after 5 h. IQE and PL mapping of PERC A show homogenously strong LeTID in good grain areas and less degradation at grain boundaries, which corresponds to previous LeTID characterization. The good grains of PERC B show hardly any IQE degradation (at mid injection) and only weak LeTID in the PL maps (at high injection). Instead, PERC B degradation is attributed to strong LeTID at recombination-active dislocation clusters. CELLO measurements show that LeTID at dislocation clusters is not only caused by increased bulk recombination, but also by increased recombination at the back surface. Therefore, the back-surface passivation appears to degrade inhomogenously during illumination at 75°C. The distribution of weak LeTID in PERC B might also be linked to the chosen surface passivation method, as lifetime samples deposited with a similar ICP-PECVD tool show low LeTID in both good grain areas and at grain boundaries.

ACKNOWLEDGMENTS

This work was partially funded by the German Federal Ministry of Economic Affairs and Energy within projects 0325763B and 0324001. J. L. thanks the Walter Ahlström Foundation for its financial support. The content is the responsibility of the authors.

REFERENCES

1. K. Ramspeck S. Zimmermann, H. Nagel, A. Metz, Y. Gassenbauer, B. Birkmann, and A. Seidl, in *Proc. of 27th EUPVSEC* (Frankfurt, Germany, 2012), pp. 861–865.
2. F. Kersten, P. Engelhart, H.-C. Ploigt, A. Stekolnikov, T. Lindner, F. Stenzel, M. Bartzsch, A. Szpeth, K. Peter, J. Heitmann, and J.W. Müller, Sol. Ener. Mat. Sol. Cells **142**, 83–86 (2015).
3. C. E. Chan, D. R. Payne, B. J. Hallam, M. D. Abbott, T. H. Fung, A. M. Wenham, B. S. Tjahjono, and S. R. Wenham, IEEE J. Photovolt. **6**, 1473–1479 (2016).
4. R. Eberle, W. Kwapil, F. Schindler, M. C. Schubert, and S. W. Glunz, Phys. Stat. Sol. RRL **10**, 861–865 (2016).
5. A. Zuschlag, D. Skorka, and G. Hahn, Prog. Photovolt. Res. Appl. **25**, 545–552 (2017).
6. T. Luka, S. Großer, C. Hagendorf, K. Ramspeck, and M. Turek. Sol. Ener. Mat. Sol. Cells **158**, 43–49 (2016).
7. F. Kersten, J. Hetimann, and J. W. Müller, Energy Procedia **92**, 828–832 (2016).
8. J. Lindroos, A. Zuschlag, D. Skorka, and G. Hahn, "Impact of surface Dielectric deposition on light-induced degradation at elevated temperature in multicrystalline silicon," IEEE J. Photovolt., submitted.
9. D. Sperber, A. Graf, D. Skorka, A. Herguth, and G. Hahn, IEEE J. Photovolt. **7**, 1627–1634 (2017).
10. J. Carstensen, A. Schütt, and H. Föll, in *Proc. of 23rd EUPVSEC* (Valencia, Spain, 2008), pp. 73–76.
11. J. Carstensen, A. Schütt, G. Popkirov, and H. Föll, Phys. Stat. Sol. C **8**, 1342–1346 (2011).
12. D. Kiliani, "Aufbau eines Lumineszenz-Messplatzes zur Charakterisierung von Solarzellen," Diploma thesis, University of Konstanz, 2009.
13. B. Fischer, "Loss analysis of crystalline silicon solar cells using photoconductance and quantum efficiency measurements," Doctoral dissertation, University of Konstanz, 2003.
14. D. Kiliani, G. Micard, B. Steuer, B. Raabe, A. Herguth, and G. Hahn, J. Appl. Phys. **110**, 054508 (2011).
15. D. Kiliani , A. Herguth, G. Micard, J. Ebser, and G. Hahn, Sol. Ener. Mat. Sol. Cells. **106**, 55–59 (2012).
16. T. Niewelt, F. Schindler, W. Kwapil, R. Eberle, J, Schön, and M. C. Schubert, Prog. Photovolt. Res. Appl., early view (2017). DOI: 10.1002/pip.2954
17. M. Selinger, W. Kwapil, F. Schindler, K. Krauß, F. Fertig, B. Michl, W. Warta, and M. C. Schubert, Energy Procedia **92**, 867–872 (2016).
18. J. Lindroos, K. Petter, K. Sporleder, M. Turek. P. Pacho, and M. Rinio, Energy Procedia **124**, 99–106 (2017).
19. C. Vargas, K. Kim, G. Coletti, D. Payne, C. Chan, S. Wenham, and Z. Hamieiri, IEEE J. Photovolt. **8**, 413–420 (2018).
20. D. Skorka, A. Zuschlag, and G. Hahn, "Firing and Gettering Dependence of Effective Defect Density in Material Exhibiting LeTID," AIP Advances (Proc. of SiliconPV 2018), submitted.